Spatially and temporally distinct Ca 2+ changes in Lotus japonicus roots orient fungal-triggered signalling pathways towards symbiosis or immunity

Spatially and temporally distinct Ca^{2+} changes in *Lotus japonicus* roots orient fungal-triggered signalling pathways towards symbiosis or immunity

Filippo Binci[1], Elisabetta Offer[1], Andrea Crosino[2], Ivan Sciascia[2], Jürgen Kleine-Vehn[3,4], Andrea Genre[2], Marco Giovannetti[1,2*], Lorella Navazio[1*]

[1]Department of Biology, University of Padova, 35131 Padova, Italy

[2]Department of Life Sciences and Systems Biology, University of Torino, 10125 Torino, Italy

[3]Centre for Integrative Biological Signalling Studies (CIBSS), University of Freiburg, 79104 Freiburg, Germany

[4]Institute of Biology II, Department of Molecular Plant Physiology (MoPP), University of Freiburg, 79104 Freiburg, Germany

*Correspondence: marco.giovannetti@unito.it; lorella.navazio@unipd.it

Highlight

Ca^{2+} changes induced by different fungal signals in *Lotus japonicus* roots are characterised by two spatially and temporally separate phases, each relying on distinct genetic programs and fostering symbiotic or immunity responses.

Abstract

Plants activate an immune or symbiotic response depending on the detection of distinct signals from root-interacting microbes. Both signalling cascades involve Ca^{2+} as a central mediator of early signal transduction. In this study, we combined aequorin- and cameleon-based methods to dissect the changes in cytosolic and nuclear Ca^{2+} concentration caused by different chitin-derived fungal elicitors in *Lotus japonicus* roots. Our quantitative analyses highlighted the dual character of the evoked Ca^{2+} responses taking advantage of the comparison between different genetic backgrounds: an initial Ca^{2+} influx, dependent on the LysM receptor CERK6 and independent of the Common Symbiotic Signalling Pathway (CSSP), is followed by a second CSSP-dependent and CERK6-independent phase, that corresponds to the well-known perinuclear/nuclear Ca^{2+} spiking. We show that the expression of immunity marker genes correlates with the amplitude of the first Ca^{2+} change, depends on elicitor concentration and is controlled by Ca^{2+} storage in the vacuole. Our findings provide an insight into the Ca^{2+}-mediated signalling mechanisms discriminating plant immunity- and symbiosis-related pathways in the context of their simultaneous activation by single fungal elicitors.

Keywords: aequorin, arbuscular mycorrhizal symbiosis, calcium, cameleon, chitin oligomers, fungal signals, *Lotus japonicus*, plant immunity, root-microbe interactions.

Introduction

Plant roots come into contact with a variety of microbes in the rhizosphere and activate different transcriptional and developmental programs in response to the identification of microbe-associated molecular patterns (Verbon and Liberman, 2016; Bonhomme *et al.*, 2021; Delaux and Schornack, 2021; Chiu *et al.*, 2022). These include highly conserved microbial components such as chitin or flagellin, normally driving plant responses towards an immunity-like program (Wan *et al.* 2012; Platre *et al.*, 2022), as well as specific microbe-released signals such as Myc factors and Nod factors, two classes of diffusible chitin-based molecules that trigger root endosymbiotic programs in arbuscular mycorrhizas and legume nodulation, respectively (Choi *et al.*, 2018; Ghahremani and MacLean, 2021). Although a diverse set of plant plasma membrane receptors is involved in the perception of microbial signals in both immunity and symbiosis (Zipfel and Oldroyd, 2017), a pivotal common mediator of downstream signalling pathways is calcium. Indeed, transient increases in intracellular calcium concentration ($[Ca^{2+}]$) have been shown to be generated during plant responses to both pathogens (Ranf *et al.*, 2011; Wan *et al.*, 2012; Nars *et al.*, 2013; Keinath *et al.*, 2015; Feng *et al.*, 2019; Zhang *et al.*, 2021, Köster *et al.*, 2022) and symbionts (Navazio *et al.*, 2007; Capoen *et al.*, 2011; Genre *et al.*, 2013; Feng *et al.*, 2019; Zhang *et al.*, 2021). Such Ca^{2+}-mediated signals encode subtle and not fully elucidated differences (the so-called Ca^{2+} signature) that are believed to control downstream activation of the appropriate molecular, cellular and metabolic responses (Zipfel and Oldroyd, 2017). In this frame, crosstalks and overlaps between microbe-released molecules, receptor roles and Ca^{2+}-mediated signal transduction pathways have been highlighted in plant symbiotic and pathogenic interactions (Ried *et al.*, 2019; Zhang *et al.*, 2021).

In this research, we focused on arbuscular mycorrhizal (AM) symbiosis, the most ancient and widespread root endosymbiosis established between the vast majority of land plants and

Glomeromycotina fungi (Choi *et al.*, 2018; Genre *et al.*, 2020). AM fungi-released Myc factors include short-chain chitin oligomers (COs), such as tetrameric chitooligosaccharides, or CO4, and lipochitooligosaccharides (mycLCOs) with structural similarities to rhizobial Nod factors (Maillet *et al.*, 2011; Genre *et al.*, 2013; Feng *et al.*, 2019). The recognition of Nod and Myc factors and the activation of the respective symbiotic programs rely on the Common Symbiotic Signalling Pathway (CSSP), encompassing a diverse set of co-receptors (LjSYMRK/MtDMI2), cation channels (LjCASTOR/MtDMI1, LjPOLLUX, MtCNGC15), Ca^{2+} transporters (MtMCA8) and Ca^{2+} sensor proteins (LjCCaMK/MtDMI3) (Charpentier, 2018; Choi *et al.*, 2018; Radhakrishnan *et al.*, 2020). Nevertheless, the cell wall of AM fungi - like all fungi - contains a large amount of long-chain chitin, a well-known pathogen-associated molecular pattern (PAMP) eliciting immunity-related responses in plants. For this reason, a number of recent studies have investigated the role of different chitin-based molecules in AM signalling, with sometimes contrasting results, likely depending on the experimental setup. While, for example, short-chain (but not long-chain) chitooligosaccharides were shown to trigger AM-specific Ca^{2+}-based symbiotic signals (Genre *et al.*, 2013), a different study suggested that octameric COs (CO8) trigger both pathogenic and symbiotic signalling (Feng *et al.*, 2019). This ambiguity is also due to our limited understanding of the complexity of signal exchange during early plant-microbe interactions and the role of plant receptors and co-receptors in different interactions and different plant species (Yu *et al.*, 2017; Zhang *et al.*, 2021). Indeed, the rice chitin receptor *OsCERK*1 was demonstrated to be crucial for both AM symbiosis and immunity (Zhang *et al.*, 2015, Miyata *et al.*, 2014, Carotenuto *et al.*, 2017) and recent research has demonstrated that the distinction between the two responses depends on the competition between two alternate co-receptors for interacting with OsCERK1 in the presence of different ligands (Zhang *et al.*, 2021). The scenario is even more complex in legumes, where the family of

LysM receptor-like kinases (which include the receptors for chitin-based signals) is much more expanded than in other plants. In *Lotus japonicus*, *LjCERK*6 is responsible for chitin-triggered immunity in response to fungal pathogens (Bozsoki *et al.*, 2017) but the corresponding receptors involved in AM symbiosis remain elusive (Chiu *et al.*, 2020). The emerging picture, given by a variable mixture of fungal signals and the overlapping roles of plant plasma membrane receptors, suggests an intricate continuum between plant immunity and symbiosis (Zhang *et al.*, 2021).

A second level of confounding factors derives from the use of distinct methodological approaches to the analysis of Ca^{2+}-mediated plant responses (Costa *et al.*, 2018; Grenzi *et al.*, 2021). On one hand, intracellular Ca^{2+} elevations in response to the perception of different PAMPs have largely been measured by using the bioluminescent genetically encoded calcium indicator (GECI) aequorin (Ranf *et al.*, 2011; Monaghan *et al.*, 2015), which provides a precise quantification of average $[Ca^{2+}]$ on whole plant or organ scale. On the other hand, CO- and LCO-triggered oscillations in perinuclear and nuclear Ca^{2+} concentrations (the so-called Ca^{2+} spiking) have been imaged at the single-cell level with the use of fluorescent GECIs, such as cameleon or GECO (Genre *et al.*, 2013; Kelner *et al.*, 2018; Feng *et al.*, 2019; Zhang *et al.*, 2021) that - unlike aequorin - do not generate absolute quantitative data. This has largely hampered the possibility of a direct comparison between the two sets of results. Few significant exceptions anyway exist: flagellin- and chitin-induced cytosolic Ca^{2+} elevations previously recorded using aequorin-based approaches revealed in fact an oscillatory nature when analysed with Yellow Cameleon 3.6 or GECO (Thor and Peiter, 2014, Keinath *et al.*, 2015). Furthermore, a single, broad elevation in cytosolic $[Ca^{2+}]$ was recorded using both approaches in response to symbiotic microbial signals (Miwa *et al.*, 2006; Navazio *et al.*, 2007) and, in the case of legume nodulation, that Ca^{2+} oscillation was found to be required for symbiosis development (Morieri *et al.*, 2013). In short, a combined

integration of qualitative (Ca^{2+} imaging) and quantitative (Ca^{2+} measurement) approaches is needed to disentangle the complexity of Ca^{2+}-mediated plant responses to biotic signals.

In this work, we analysed the effects induced by a set of chitin-related oligomers on cytosolic and nuclear Ca^{2+} levels in different genetic backgrounds of *L. japonicus* roots by targeting aequorin-based Ca^{2+} reporters to distinct cellular compartments. We accurately quantified the Ca^{2+} signatures associated with individual fungal molecules and showed that CO4-, CO8- and mycLCO-induced Ca^{2+} elevations differ in their intracellular localization, temporal dynamics and plant genetic requirements. A complementary approach based on Ca^{2+} imaging with a nuclear-localized cameleon probe in *Medicago truncatula* root organ cultures further supported our dissection of the observed plant root Ca^{2+} responses in two distinct temporal phases, also highlighting a dependency on elicitor concentration. The resulting insight in the communication circuits that plants and microbes develop in the rhizosphere advance our quantitative understanding of how roots discriminate against different fungal molecules, activating the appropriate symbiotic or defence responses downstream.

Materials and Methods

Molecular cloning and bacterial transformation

The nucleotide sequence encoding the bioluminescent Ca^{2+} indicator aequorin fused to Yellow Fluorescent Protein (YFP) and targeted to either the cytosol-only ($CPK17_{G2A}$-NES-YA) or nucleus-only (NLS-YA) (Mehlmer *et al.*, 2012) were amplified with Q5 DNA polymerase (NEB) according to manufacturer's instructions. The promoter (1100 bp upstream of the ATG) of Ubiquitin-10 was amplified from the genome of *Lotus japonicus* (Gifu ecotype). Primers (listed in Table S1) were designed to be compatible with the GreenGate cloning system and cloning of the entry vectors was performed according to it

(Lampropoulos *et al.*, 2013). Expression vectors were assembled via cut-ligation with BsaI (NEB) and T4-DNA ligase (NEB), following the GreenGate protocol. The selection and amplification of vectors were performed in DH5α *E. coli* cells. The sequences were checked via Sanger sequencing at BMR Genomics (Padova, Italy) and by Primordium long-read DNA sequencing at Primordium Labs (Arcadia, CA, USA). The expression vectors were then transformed into *Agrobacterium rhizogenes* 1193 via the freeze & thaw method (Wise *et al.*, 2006). Expression vectors are listed in Table S2.

Generation of Lotus japonicus composite plants

L. japonicus Gifu wild-type, *symrk-3*, *castor-1*, and *cerk6-1* (Małolepszy *et al.*, 2016; Mun *et al.*, 2016; Bozsoki *et al.*, 2017) seeds were scarified with sandpaper and sterilized in 0.5% (w/v) sodium hypochlorite for 11 min. Seeds were then rinsed and washed 5 times in sterile distilled water. For germination, seeds were placed into sterile Petri dishes with H_2O with 1% (w/v) plant agar and wrapped in aluminum foil. After 3 days at 23°C, young seedlings were transferred to square plates (12x12 cm) containing ½ strength B5 growth medium, supplemented with 0.8% (w/v) plant agar and adjusted to pH 5.5 with 1 M KOH. Plates were grown vertically under long-day conditions (23°C, 16 h light/8 h dark cycle). After 3 days, the seedlings were transformed via *A. rhizogenes 1193* - mediated hairy root transformation (Boisson-Dernier *et al.*, 2001). The root was cut off with a blade and the wound was dipped into a fully grown plate of *A. rhizogenes* carrying the plasmid of interest. The infected shoots were then placed onto square plates (12x12 cm) containing ½ strength B5 growth medium, 0.8% plant agar, pH 5.5. After 16 h in the darkness, seedlings were co-cultivated with bacteria for 3 days. Afterward, the seedlings were transferred into new squared plates with the same medium supplemented with 300 µg/ml cefotaxime and 0.1% (v/v) Plant Preservative Mixture (PPM, Duchefa) under long-day conditions (16 h light/8 h dark cycle) at

23°C. After 3 weeks, transformed roots were checked for expression of the transformation marker (pAtUBQ10::mCherry) using the stereomicroscope MZ16F (Leica). The intracellular localization of the probe was confirmed by confocal microscopy observations (Zeiss LSM900 Airyscan2). Transformed plants were kept in the same growth medium under long-day conditions.

Aequorin-based Ca^{2+} measurement assays

For Ca^{2+} measurement assays in *L. japonicus* composite plants, 5 mm segments of transformed roots expressing aequorin targeted to either the cytosol or nucleus were reconstituted overnight with 5 µM coelenterazine. On the following day, after extensive washing, each root piece was placed in the dark chamber of a custom-built luminometer (Electron Tubes) containing a 9893/350A photomultiplier (Thorn EMI). The root was placed in 50 µl H_2O and challenged by injection of an equal volume of a 2-fold concentrated solution for each tested stimulus: CO4, CO8 (IsoSep), mycLCOs (equimolar mix of both non-sulfated and sulfated C16:0 and C18:1). The stock solutions were 10^{-3} M in 50% ethanol for CO4, 10^{-4} M in 50% ethanol for CO8, 10^{-3} M in DMSO for mycLCOs. Controls were performed by injecting an equal volume of the solvents in which the compounds were dissolved at the working concentration. Ca^{2+} dynamics were recorded for a total of 30 min before the injection of 100 µl discharge solution (30%, v/v, ethanol, 1 M $CaCl_2$). The light signal was collected and converted offline into Ca^{2+} concentration values using a computer algorithm based on the Ca^{2+} response curve of aequorin (Brini *et al.*, 1995). All Ca^{2+} concentration values for each biological replicate are available (Table S3). For pharmacological analyses, the root pieces, before challenge with chito-oligomers, were pre-treated with the pharmacological agents for different time intervals: 1.5 mM $LaCl_3$ (Sigma) and 2 mM EGTA (Sigma) for 10 min, 50 µM cyclopiazonic acid (CPA, stock solution 30

mM in DMSO) for 1 h, 10 µM VAC1 (stock solution 10^{-3} M in DMSO) for 2.5 h (Dünser *et al.*, 2022).

Cameleon-based Ca^{2+} imaging assays

Medicago truncatula genotype Jemalong A17 were genetically transformed using *A. rhizogenes* to generate root organ cultures expressing the nuclear-localized 35S:NupYC2.1 cameleon construct (Sieberer *et al.*, 2009), as described by Chabaud *et al.* (2011). Ca^{2+} imaging was conducted on excised young lateral roots, placed in 2 mm-thick microscope slide microchambers. The water in the microchamber was rapidly (< 30 s) substituted by 200 µl of CO4 solution before initiating confocal image acquisition within 1-3 minutes. 8 independent root samples were used to record 30-min-long Ca^{2+} traces from at least 9 atrichoblasts each. FRET-based ratio imaging of the YFP and CFP cameleon fluorescence was used for the detection and plotting of relative changes in nuclear Ca^{2+} levels (Chabaud *et al.*, 2011).

Gene expression analysis

L. japonicus Gifu seeds were sterilized as described above and the seedlings were grown for 10 days (16 h light/8 h dark cycle at 23°C) in vertical square plates (12x12 cm) containing ½ strength B5 growth medium, 0.8% (w/v) agar, pH 5.5. Groups of 12 plants were treated in 4 ml solutions containing either 10^{-7} M CO4, 10^{-9} M CO4 or the control treatment (50% ethanol diluted 1:1000). The grouped samples were harvested after 1 h of treatment. During harvesting, roots were cut from shoots and immediately frozen in liquid N_2 in a 2 ml tube containing two metal beads. The root material was homogenized with TissueLyser II (Qiagen) at 30 Hz for 45 seconds. Total RNA was extracted using the RNeasy Plant Mini Kit (Qiagen) following the manufacturer's instructions. RNA quantity and quality were checked

by nanodrop and agarose gel electrophoresis. After DNAse I (Invitrogen) treatment, cDNA synthesis was performed with random hexamers using the RevertAid RT Kit (Thermofisher). qRT-PCR was performed using the HOT FIREPOL EvaGreen qPCR mix plus (Solis Biodyne) on a 7500 real-time PCR system (Applied Biosystems). The *LjUbiquitin10* and *LjATP synthase* genes were used as an internal reference for analysis of the target gene expression. All the primers (Table S1) used for the qRT-PCR analyses have been previously published (Nakagawa *et al*., 2011; Giovannetti *et al*., 2015; Bozsoki *et al*., 2017).

Statistical analysis and data visualisation

Data were statistically analysed and presented graphically using R statistical environment and Rstudio (RStudio Team, 2020; R Core Team, 2022). When passing its assumptions, the Anova test and Tukey's post-hoc test was applied; in the other cases, Kruskal Wallis and Dunn's tests were performed (Table S3). R scripts (Supplementary Dataset S1) and raw data (Supplementary Dataset S2-S8) ensure full reproducibility of statistical analyses and plots.

Results

Reexamining plant cytosolic and nuclear Ca^{2+} changes in response to different fungal signals reveals common and unique features

In the field of plant symbioses, numerous studies have relied on the use of fluorescent GECIs (mainly cameleon) to finely image [Ca^{2+}]; however, the bioluminescent Ca^{2+} reporter aequorin is among the most reliable tools when accurate measurements of [Ca^{2+}] variations during signal transduction are needed (Costa *et al*., 2018; Greotti and De Stefani, 2020). We therefore chose to use this Ca^{2+}-sensitive photoprotein to quantify Ca^{2+} changes in *L. japonicus* roots treated with different fungal signals. To this aim we assembled expression cassettes for YFP-tagged aequorin-based chimeras specifically targeted to either the cytosol

or the nucleus (Mehlmer *et al.*, 2012) under the control of the *LjUBI10* promoter and the correct localization of the Ca^{2+} probe was confirmed by confocal imaging of YFP (Supplementary Fig. S1). Root segments from *L. japonicus* composite plants were then challenged with the purified fungal signals CO4 (short-chain COs), CO8 (long-chain COs) and mycLCOs (using a mixture of sulfated and non-sulfated molecules), and the changes in intracellular [Ca^{2+}] were measured. All categories of chitin-based oligomers were found to trigger cytosolic Ca^{2+} changes of varying intensity and timing (Fig. 1A,C, Supplementary Fig. S2, Table S3 and Dataset S2). In particular, 10^{-7} M CO4 induced cytosolic Ca^{2+} transients with the highest peak magnitude, while a more reduced peak amplitude was recorded upon myc-LCO treatment at the same concentration. Notably, a 10^{-6} M concentration of CO8 was necessary to trigger a Ca^{2+} change of comparable amplitude. No Ca^{2+} changes were recorded upon administration of solvent controls (Fig. 1A and Dataset S2).

For all treatments, the overall shape of the observed cytosolic Ca^{2+} dynamics appeared markedly biphasic, with an initial major peak recorded in the first 8 minutes after stimulation, followed by a broader shoulder. Such dynamics closely resemble those triggered by germinating spore exudates of *Gigaspora margarita* in soybean (Navazio *et al.*, 2007) or *L. japonicus* cultured cells (Moscatiello *et al.*, 2018).

Furthermore, CO4, mycLCOs, and CO8 also induced Ca^{2+} transients in the nucleus (Fig. 1B,D) apparently lacking the initial sharp peak when compared to cytosolic traces. In fact, statistical analysis did not reveal any significant difference in either the overall shape or total mobilized Ca^{2+} for the nuclear-induced transients triggered by the three microbial signals (Fig. 1, Supplementary Fig. S2 and Table S3), all of which are known to activate nuclear Ca^{2+} responses in cameleon-based assays (Genre *et al.*, 2013; Sun *et al.*, 2015; Feng *et al.*, 2019).

Based on this initial overview, Ca^{2+} transients activated by the three fungal signals displayed similar features, i.e. comparable timing, a marked biphasic pattern in the cytosol and a sustained elevation in the nucleus. In order to further investigate whether such an apparent similarity could subtend biologically relevant differences in Ca^{2+} sources and/or molecular determinants, we designed a number of pharmacological and genetic analyses.

Extracellular, vacuolar and endoplasmic reticulum-associated Ca^{2+} pools differentially contribute to shaping cytosolic and nuclear Ca^{2+} signals

To elucidate the source of the observed nuclear and cytosolic Ca^{2+} fluxes activated by chitin oligomers we performed a pharmacological analysis, focusing on CO4, *i.e.* the symbiotic signals that triggered the most striking [Ca^{2+}] changes when applied at the lowest concentration. Firstly, in order to assess the contribution of extracellular Ca^{2+} to the generation of the observed Ca^{2+} responses, we pretreated roots with either the Ca^{2+} channel inhibitor $LaCl_3$ or the extracellular chelator EGTA. $LaCl_3$ treatment caused a complete abolishment of the Ca^{2+} response to CO4 in both the cytosol (Fig. 2A,C, Table S3 and Dataset S3) and nucleus (Fig. 2B,D and Table S3). The cytosolic Ca^{2+} trace was almost completely flattened also in the presence of EGTA, where the main peak of the first phase (within 8 min after the stimulus, hereafter called phase 1) was replaced by a very limited Ca^{2+} elevation (Fig. 2A,C and Table S3). Notably, in the presence of EGTA, a short Ca^{2+} transient of regular amplitude was maintained in the first 8 minutes of nuclear traces (Fig. 2B,D and Table S3), whereas [Ca^{2+}] dropped to resting levels 8-30 min after the stimulus (hereafter called phase 2). These observations suggest that chelation of extracellular Ca^{2+} has a significant impact on phase 1 Ca^{2+} signalling in the cytosol, but not the nucleus.

In order to investigate the contribution of intracellular Ca^{2+} stores to the generation of the observed signals, we then misregulated Ca^{2+} homeostasis in the endoplasmic reticulum (ER)

and vacuole. To this aim, we applied either cyclopiazonic acid (CPA), an inhibitor of ER-type Ca^{2+} ATPases causing Ca^{2+} depletion of the ER lumen (De Vriese *et al.*, 2018; Cortese *et al.*, 2022), or VAC1, an inhibitor of SNARE-dependent vesicle fusions causing an overall reduction in vacuole size (Dünser *et al.*, 2022) and Ca^{2+} storage capability.

Pretreatment with CPA did not alter the phase 1 peak in the CO4-induced cytosolic Ca^{2+} elevation (Fig. 2A,C and Table S3), suggesting that the ER is not involved in the generation/dissipation of the Ca^{2+} fluxes contributing to this phase. By contrast, CPA completely abolished the Ca^{2+} transient in the nucleus (Fig. 2B,D and Table S3); this is consistent with the predicted role played by the nuclear envelope - which is in continuity with the ER - as a major source for nuclear and perinuclear Ca^{2+} spiking (Capoen *et al.*, 2011). Notably, CPA caused a statistically significant increase in the basal level of $[Ca^{2+}]$ in ~~both~~ the cytosol (Fig. 2A and Table S3) and the same trend is visible in the nucleus (Fig. 2B), in line with the role of the plant ER in Ca^{2+} homeostasis.

By contrast, pre-treatment of *L. japonicus* roots with VAC1 strongly reinforced phase 1 cytosolic Ca^{2+} peak in response to CO4 (Fig. 2A,C), suggesting that VAC1-dependent alterations in vacuolar function reduced Ca^{2+} uptake from the cytosol. Conversely, the nuclear Ca^{2+} transient was largely unaffected in VAC1-treated roots (Fig. 2B,D and Table S3), indicating that the vacuole has a minor (if any) role in nuclear symbiotic Ca^{2+} signals. Beside demonstrating the role of the ER in the generation of nuclear Ca^{2+} changes in response to CO4, these results uncover a previously neglected contribution of the vacuole in shaping CO4-induced cytosolic Ca^{2+} fluxes.

Ca^{2+} measurements in L. japonicus CSSP mutant backgrounds corroborate the biphasic nature of the intracellular Ca^{2+} signatures triggered by chitin-derived oligomers

To further dissect the intracellular Ca^{2+} signals in *L. japonicus* roots in response to chitin-derived molecules, we compared our analyses in wild-type *L. japonicus* and two mutants for genes that are essential for the progression of the Common Symbiotic Signalling Pathway (or CSSP; Oldroyd, 2013; Choi *et al.*, 2018; Radhakrishnan *et al.*, 2020): *LjSYMRK*, encoding a plasma membrane co-receptor, and *LjCASTOR*, encoding a nuclear cation channel.

Phase 1 of the cytosolic Ca^{2+} transient was found to be maintained in both CSSP mutants, but with relevant distinctions: firstly, the CO4-induced peak was significantly reduced in *castor* compared to both the wild-type and *symrk* (Supplementary Fig. S3A-B, Dataset S4 and Table S3). Secondly, the CO8-induced cytosolic Ca^{2+} peak showed a mild, although statistically not significant, increase in both *symrk* and *castor*, compared to the wild-type (Supplementary Fig. S3E-F and Table S3). Lastly, no differences could be identified in the mycLCO-induced cytosolic Ca^{2+} peak in phase 1 (Supplementary Fig. S3I-J and Table S3). Concerning cytosolic phase 2, a slight - albeit statistically not significant - reduction in Ca^{2+} elevation was detected in response to both CO4 and mycLCOs in the two CSSP mutants compared to the wild-type. By contrast, cytosolic Ca^{2+} traces in response to CO8 were largely superimposable among all three genotypes (Supplementary Fig. S3 and Table S3).

More relevant differences between *L. japonicus* genetic backgrounds appeared when we compared nuclear Ca^{2+} transients (Fig. 3, Dataset S4 and Table S3). While in fact the initial and steep increase in nuclear [Ca^{2+}] triggered by the three stimuli was retained in *symrk* and *castor* mutants, the broad, dome-shaped Ca^{2+} elevation of phase 2 was absent in CO4- and mycLCO-treated mutants, but only weakly reduced upon CO8 application. This is further supported by the quantification of mobilised Ca^{2+} in terms of integral [Ca^{2+}] and time

duration of the response above an arbitrary [Ca^{2+}] threshold (width) (Fig. 3A-D, I-L and Table S3).

Together, these results provide several important clues. Firstly, they suggest that a functional CSSP is dispensable for the cytosolic Ca^{2+} influx of phase 1, even if it appears to modulate it. Secondly, the CSSP dependency of nuclear (and partially cytosolic) Ca^{2+} elevation in phase 2, echoes the lack of nuclear and perinuclear Ca^{2+} spiking described in literature for mutants of the corresponding orthologous genes in *M. truncatula* (Genre *et al.*, 2013; Feng *et al.*, 2019).

Supporting the hypothesis that aequorin-based Ca^{2+} traces are the sum of Ca^{2+} spiking signals from a population of individual cells

The interpretations of aequorin-based Ca^{2+} transients as the sum of individual and non-synchronous Ca^{2+}-spiking events in single root cells (described using fluorescent GECIs) had previously been advanced (Genre *et al.*, 2013; Kelner *et al.*, 2018; Feng *et al.*, 2019). Anyway, our detailed dissection of Ca^{2+} traces into a CSSP-independent (and vacuole-modulated) Ca^{2+} influx in phase 1, and a CSSP-dependent, ER-generated nuclear Ca^{2+} elevation in phase 2, now allowed us to test this hypothesis.

To this aim, a complementary set of experiments was conducted, based on the recombinant expression of the fluorescent Ca^{2+} probe NupYC2.1 in *Medicago truncatula* root organ cultures, a commonly used and easy to manipulate experimental system for studying Ca^{2+} spiking in AM interactions (Chabaud *et al.*, 2011; Genre *et al.*, 2013; Volpe *et al.*, 2020). When challenged with 10^{-7} M CO4, root atrichoblasts displayed a cell-autonomous range of Ca^{2+}-spiking signals (Fig. 4A,B, Supplementary Fig. S4 and Dataset S5), in line with literature data (Genre *et al.*, 2013). In more detail, responding cells typically displayed an early elevation in [Ca^{2+}] of variable height, shape and duration, but always included within

the first 8 minutes from treatment. Subsequently, a series of peaks in [Ca^{2+}] appeared, also in this case with a very broad variability in terms of peak number, frequency and regularity.

In order to compare this cameleon-based, single cell imaging of nuclear Ca^{2+} oscillations with aequorin-based whole-root analyses, we generated average Ca^{2+} traces combining the signals acquired from all responding cells for each root and a polynomial curve fitting data points of the resulting average Ca^{2+} trace was calculated for each root (Fig. 4C,D and Dataset S1). The resulting curves showed an initial Ca^{2+} elevation during the first 8 minutes after stimulus application, followed by a second, broader shoulder. This resemblance to the traces obtained with the aequorin-based analyses of nuclear [Ca^{2+}] appears particularly remarkable if one considers that we were comparing different plant species. In short, this extra-experiment and the elaboration of a population of raw spiking traces, offered sufficient support for the hypothesis that whole-root records generated with recombinant aequorin indeed correspond to the sum of a population of individual Ca^{2+} spiking signals.

The LysM receptor CERK6 is essential for the induction of the phase 1 peak in cytosolic and nuclear Ca^{2+} in response to short- and long-chain chitin oligomers

Our combined use of drug treatments and *L. japonicus* CSSP mutants resulted in the elimination of either the entire Ca^{2+} response to CO4 and CO8 (Fig. 2) or phase 2 alone (Fig. 3), but not phase 1 alone. Since a steep cytosolic Ca^{2+} influx is known to play a crucial role in plant immunity (Ranf *et al.*, 2012; Monaghan *et al.*, 2015; Kutschera *et al.*, 2019; Thor *et al.*, 2020), we decided to investigate whether we were observing this very signalling process. We therefore analysed Ca^{2+} responses to COs in *L. japonicus cerk6* mutant background. CERK6 is a LysM receptor kinase with high affinity for fungal-derived and purified COs, that is required for mounting plant immunity response (Boszoki *et al.*, 2017 and 2020). In our hands, CO4 and CO8-induced cytosolic and nuclear Ca^{2+} signals were partially impaired in *cerk6*

mutants, compared to wild-type and *symrk* lines (Fig. 5 and Dataset S4). In particular, all responding *cerk6* plants showed a Ca^{2+} transient, the timing of which was compatible with the preservation of phase 2 alone. Importantly, however, only around 30% of *cerk6* root segments produced Ca^{2+} signals in response to CO treatments, compared to close to 100% responsiveness in wild-type, *symrk* and *castor* backgrounds. The dependency of phase 1 Ca^{2+} peak on CERK6 convincingly supports the hypothesis that it corresponds to the well-known defence-associated Ca^{2+} influx. We can therefore conclude that aequorin-based Ca^{2+} traces in response to CO perception combine a CERK6-dependent, CSSP-independent peak during phase 1, resulting from a major Ca^{2+} influx from the apoplast, and a less prominent, CERK6-independent, CSSP-dependent elevation during phase 2, corresponding to nuclear/perinuclear Ca^{2+}-spiking.

Fungal elicitor concentration affects the amplitude of phase 1 Ca^{2+} elevation and the activation of immunity marker genes

It has previously been demonstrated that the intensity of intracellular Ca^{2+} changes in response to rhizobial Nod factors (Shaw and Long, 2003) and AM fungal exudates (Chabaud *et al.*, 2011) are concentration-dependent. To test if this was also the case for fungal COs, we monitored cytosolic and nuclear Ca^{2+} signals in *L. japonicus* roots challenged with serial dilutions of CO4 and CO8 (Fig. 6, Supplementary Fig. S5 and Dataset S6). Concerning cytosolic signals, we found that while the amplitude of phase 1 Ca^{2+} peak strongly depends on both CO4 and CO8 concentration, phase 2 was not apparently affected by the working dilutions. In more detail, 10^{-6} M and 10^{-7} M CO4 produced comparable traces, suggesting that the system is already saturated at 10^{-7} M. In the nucleus, by contrast, phase 1 Ca^{2+} peak did not change between 10^{-8} M and 10^{-6} M CO4 treatments. Moreover, 10^{-9} M CO4 did not trigger any visible response in the cytosol, while the nuclear phase 2 Ca^{2+} elevation persisted

(Fig. 6A-B). In line with these observations, the treatment of NupYC2.1-expressing *M. truncatula* root organ cultures with 10^{-9} M CO4 resulted in nuclear Ca^{2+} traces that often lacked phase 1 Ca^{2+} peak (Supplementary Fig. S6 and Dataset S7) but retained phase 2 Ca^{2+} spiking, albeit overall less pronounced than upon 10^{-7} M CO4 treatment (Fig. 4).

To further investigate the physiological relevance of phase 1 Ca^{2+} peak and its possible link with the induction of plant defence responses, we tested to what extent 10^{-7} M and 10^{-9} M CO4 triggered the expression of immunity marker genes *LjChitinase*, *LjRbohB-like*, *LjWRKY70-like*, *LjPRp27-like*. These four genes have previously been shown to be activated by 10^{-6} M CO4 and CO8 in a CERK6-dependent manner (Bozsoki *et al.*, 2017). Indeed, 10^{-7} M CO4 triggered the expression of all four immunity markers after 1 h treatment. By contrast, 10^{-9} M CO4 failed to activate the selected defence markers, with the only exception of a slight but not statistically significant induction of *PRp27-like* (Fig. 6E and Supplementary Dataset S8). Intriguingly, according to LotusBase ExpressionAtlas (Mun *et al.*, 2016; Kamal *et al.*, 2020), *LjPRp27-like* shows a peculiar expression pattern with strong and specific gene activation in both Ralstonia-infected plants and AM-colonised roots (Supplementary Fig. S7). This expression profile is unique among the tested immunity marker genes (Lotus Base) and could provide an explanation for the upregulation of *LjPRp27-like* by 10^{-9} M CO4. Altogether, these results are consistent with our interpretation of a biphasic nature in such Ca^{2+} signals and indicate a dose-dependent regulation of both Ca^{2+}-mediated signalling and immunity-related gene expression.

DISCUSSION

In this work, we identified complex and biphasic compartment-specific Ca^{2+} signatures activated in response to different fungal signals in *L. japonicus* roots. Aequorin-based Ca^{2+} measurement assays demonstrated that short-chain (CO4), long-chain (CO8) and lipidated (mycLCOs) chitooligosaccharides can all induce both cytosolic and nuclear Ca^{2+} transients,

that we were able to dissect in two different temporal phases and ascribe them to diverging defence- and symbiosis-related signalling pathways. Our findings on AM signalling provide insights into specific features of Ca^{2+}-mediated signals that were previously only investigated in *Rhizobium*-legume interactions (Shaw and Long, 2003; Morieri *et al.*, 2013), and outline a scenario where a clear-cut distinction between pathogenic and symbiotic fungal elicitors has to be overcome and integrated into a complex picture taking into account a combination of symbiosis- and defence-associated signalling cascades within the responding plant cells.

Extending previous reports of Ca^{2+} transients in soybean and *L. japonicus* cell cultures in response to germinating AM spore exudates (Navazio *et al.*, 2007; Francia *et al.*, 2011; Moscatiello *et al.*, 2018), our tests with three categories of AM fungal elicitors (CO4, CO8 and mycLCOs) demonstrated the onset of a steep Ca^{2+} increase in *L. japonicus* roots within the first 8 minutes after treatment (phase 1). This Ca^{2+} elevation was recorded using both cytosolic and nuclear aequorin constructs and was independent of CSSP integrity and ER-based Ca^{2+} storage, but dependent on CERK6 and the extracellular Ca^{2+} pool. Furthermore, the dynamics of such cytosolic and nuclear Ca^{2+} increases in phase 1 were compatible with those of the PAMP-triggered Ca^{2+} influx mounting plant immunity (Ranf *et al., 2013*, Zipfel and Oldroyd, 2017). These convergent results support the conclusion that the phase 1 peak is indeed a defence-related signalling process common to both symbiotic and pathogenic plant-fungus interactions, in line with the well-known early activation of a weak defence response during AM development (Giovannetti *et al.*, 2015) and previous indications that fungal elicitors activate multiple parallel signalling cascades (Bonfante and Requena, 2011). This is further supported by the observed activation of immunity marker genes by 10^{-7} M CO4 treatment (which induced the phase 1 Ca^{2+} elevation), but not 10^{-9} M CO4 treatment (where the same Ca^{2+} change was not recorded). Intriguingly, the use of VAC1, a recently developed

drug reducing vacuole size (Dünser *et al.*, 2022), hinted at the involvement of this extensive and multifunctional cell compartment in the dissipation of phase 1 Ca^{2+} rise. Future applications of the newly designed aequorin-based (Cortese *et al.*, 2022) and GCaMP-based (Luo *et al.*, 2020; Resentini *et al.*, 2021) probes targeted to the plant ER, possibly alongside yet-to-develop GECIs for vacuolar Ca^{2+} measurement/imaging, will be crucial to clarify the exact contribution of each organelle to shaping symbiotic Ca^{2+} signalling.

Moreover, we observed phase 2 Ca^{2+} responses in the absence of phase 1, either upon the administration of very low concentrations of the fungal elicitors or in the *cerk6* mutant. Similarly, Nod factor-induced Ca^{2+} influx in *M. truncatula* root hairs has previously been shown to be independent of the CSSP, but dependent on the Nod factor dose (Shaw and Long, 2003) and chemical structure (Morieri *et al.*, 2013). However, we cannot exclude a role for CERK6 also in symbiotic signalling. Indeed, the absence of a mycorrhizal phenotype in the *cerk6* mutant has previously been observed at a single time point (Bozsoki *et al.*, 2017), whereas a deeper analysis in the *MtLyk9* mutant (the putative CERK6 closest homolog in *M. truncatula*) has shown a weak reduction in AM colonization compared to wild-type plants (Feng *et al*., 2019; Gibelin-Viala *et al*., 2019). Accordingly, about two-third of the *cerk6* root samples tested in our assays did not respond with a clear activation of phase 2 Ca^{2+} elevation.

Experiments using pharmacological pretreatments and different genetic backgrounds highlighted a number of common features between the prolonged Ca^{2+} elevation detected in phase 2 by the aequorin-based analyses and the Ca^{2+} spiking events recorded with fluorescent GECIs (Genre *et al.*, 2013; Kelner *et al*., 2018; Feng *et al*., 2019) in response to CO treatments. Such common features include overlapping temporal dynamics, CSSP dependency and the involvement of the nuclear envelope as the intracellular Ca^{2+} source (Zipfel and Oldroyd, 2017; Charpentier, 2018).

We also propose that the phase 2 Ca^{2+} cytosolic elevation present in our aequorin-based analyses corresponds to perinuclear Ca^{2+} spiking, which is known to be simultaneous with nuclear Ca^{2+} spiking (Ehrhardt *et al.*, 1996; Kelner *et al.*, 2018). The low amplitude of this cytosolic Ca^{2+} transient may be due to the fact that the aequorin chimera ($CPK17_{G2A}$-NES-YA) used in this work provides a measure of [Ca^{2+}] changes in the bulk cytosol (Mehlmer *et al.*, 2012; Ottolini *et al.*, 2014), rather than at microdomains close to the nuclear envelope, as highlighted in detail by cameleon or GECO-based Ca^{2+} imaging.

Despite being widely considered as canonical fungal PAMPs (Cao *et al.*, 2014; Bjornson *et al.*, 2021), CO8 have recently been suggested to also act as symbiotic molecules and activate both nuclear Ca^{2+} spiking and the expression of symbiotic genes (Feng *et al.*, 2019, Zhang *et al.*, 2021). In our experimental setup, CO8 activated a nuclear phase 2 Ca^{2+} response in the wild-type background, apparently similar to the CO4- and mycLCOs-induced ones. However, this response was not statistically significantly dependent on SYMRK and CASTOR, highlighting that CO8-induced Ca^{2+} signalling also underlies transduction pathways unrelated to symbiosis. In the light of this observation, it will be interesting to investigate in more detail CO8-triggered nuclear Ca^{2+} signals and their similarities and differences with CO4 and LCO-induced spiking.

Recent literature has suggested a cross-talk between immunity and symbiosis signalling pathways upon plant perception of root endosymbionts. In this scenario, the prevalence of either pathway depends on a combination of elicitors, receptor competition and cross-reactions among players of the activated signalling cascades (Feng *et al.*, 2019, Zhang *et al.*, 2021, Feng *et al.*, 2021) and the trade-off between accommodation and defence is finely tuned by the plant during AM colonization. Here, we suggest that the boundaries between *bona-fide* pathogenic and symbiotic fungal signals are less clear-cut than previously thought, since all the tested molecules could activate parallel pathways that converge in multi-phasic

Ca^{2+} signals. Indeed, we dissected independent components of the Ca^{2+} responses based on timing, genetic background and elicitor concentration. Moreover, we correlated the activation of immunity marker genes with the presence of phase 1 Ca^{2+} influx, suggesting that the dose of chitin-derived molecules plays a key role in the activation of different plant responses to root-interacting microbes.

By carefully comparing data coming from *L. japonicus* roots expressing nuclear aequorin and nuclear-targeted cameleon in *M. truncatula* root organ cultures, we were able to depict a correspondence between the two datasets, eventually leading to significant insights into plant symbiotic signalling. On the one hand, we confirmed the occurrence of a rapid Ca^{2+} change in response to CO4 perception during phase 1. This initial Ca^{2+} elevation induced by short-chain chitin oligomers is recognizable in published Ca^{2+} traces obtained with cameleon-based technique, but has long been overlooked, most likely because of its fast and irregular occurrence, and analogous Ca^{2+} elevations in response to Nod factor perception have only been investigated in a limited number of studies (Shaw and Long., 2003; Morieri *et al.*, 2013). In this frame, our results bring this elusive element of Ca^{2+}-mediated symbiotic signalling back in the spotlight, hopefully fostering new research in this field. Our data show that a combination of cameleon-based Ca^{2+} traces from individual root epidermal cells does mimic the overall dynamics of this initial CO4-induced Ca^{2+} transient as recorded using aequorin, but cannot fully reproduce its kinetic parameters, suggesting that a much larger number of individual traces should be merged, or additional cell layers (*e.g.* belonging to the root cortex), may contribute to the global root Ca^{2+} response to COs observed by recording aequorin-dependent light emission from whole roots. On the other hand, the combination of two Ca^{2+} monitoring methods in different plant species provided convincing support to our interpretation of phase 2 Ca^{2+} elevation as the sum of individual nuclear Ca^{2+}-spiking signals.

The evident similar features in aequorin-based and averaged cameleon-based Ca^{2+} traces allows a direct comparison between the results obtained with these commonly used and complementary approaches. This possibility encourages the re-evaluation of literature data, fruitful synergies in future projects, including aequorin-based chemical screenings (Yao *et al.*, 2022) or high-throughput genetic screenings - so far mainly limited to the plant immunity field (Tian *et al.*, 2019; Mittal *et al.*, 2020; Wu *et al.*, 2020) - and, hopefully, innovative intuitions unravelling the intricacy of Ca^{2+}-mediated symbiotic signalling in plants.

Acknowledgements

We thank Ute Vothknecht (University of Bonn, Germany) for the $CPK17_{G2A}$-NES-YA and NLS-YA plasmids, Marco Incarbone and Mattia Donà (Gregor Mendel Institute, Vienna, Austria) for the destination vector, and Sébastien Fort (CNRS, Paris, France) for the mycLCOs. We are grateful to Lene Heegaard Madsen, Simona Radutoiu and Jens Stougaard (Aarhus University, Denmark) for kindly providing *L. japonicus symrk*, *castor* and *cerk6-1* mutants, and to Myriam Charpentier (John Innes Centre, Norwich, UK) for fruitful discussions. The technical assistance of the Imaging Facility and the Plant Genome Editing Facility of the Department of Biology (University of Padova, Italy) is gratefully acknowledged.

Author contributions

LN and MG conceived the study and designed research; FB and MG conducted molecular cloning; FB performed intracellular localization studies and gene expression analysis; FB and EO performed aequorin-based Ca^{2+} measurements; AC and FB performed cameleon-based Ca^{2+} assays; MG and FB analysed data, conducted statistical analyses and data visualisation; AC, IS and FB conducted data analysis and modelling of Ca^{2+} imaging data; FB, MG and LN wrote the article; AG designed some experiments and contributed to the discussion and editing of the article; JKV provided materials and contributed to the discussion. All authors read and approved the final manuscript.

Conflict of interest

The authors declare that they have no conflicts of interest.

Funding

This work was supported by grants from the Italian Ministry of University [PRIN 2022 - grant 2022NW97JX to LN and AG], from the University of Padova (Progetti di Ricerca Dipartimentali - PRID) [grant number BIRD180317 to LN; grant number BIRD214519 to MG; PRID Seed Giovani to FB], from the European Union - NextGenerationEU [2021 STARS Grants@Unipd programme P-NICHE to MG]), from the Austrian Science Fund (FWF) [grant number P 33044 to JK-V], and the German Science fund (DFG) [grant number 470007283 and CIBSS-EXC-2189 to JK-V].

Data availability

The datasets used in this study are available in the Supplementary data.

References

Bjornson M, Pimprikar P, Nürnberger T, Zipfel C. **2021**. The transcriptional landscape of *Arabidopsis thaliana* pattern-triggered immunity. *Nature Plants* **7**, 579–586.

Boisson-Dernier A, Chabaud M, Garcia F, Bécard G, Rosenberg C, Barker DG. **2001**. *Agrobacterium rhizogenes*-transformed roots of *Medicago truncatula* for the study of nitrogen-fixing and endomycorrhizal symbiotic associations. *Molecular Plant-Microbe Interactions* **14**, 695–700.

Bonfante P, Requena N. 2011. Dating in the dark: how roots respond to fungal signals to establish arbuscular mycorrhizal symbiosis. *Current Opinion in Plant Biology* **14**, 451-457.

Bonhomme M, Bensmihen S, André O, et al. 2021. Distinct genetic basis for root responses to lipo-chitooligosaccharide signal molecules from different microbial origins. *Journal of Experimental Botany* **72**, 4.

Bozsoki Z, Cheng J, Feng F, Gysel K, Vinther M, Andersen KR, Oldroyd GED, Blaise M, Radutoiu S, Stougaard J. 2017. Receptor-mediated chitin perception in legume roots is functionally separable from Nod factor perception. *Proceedings of the National Academy of Sciences*, USA **114**, 8118-8127.

Bozsoki Z, Gysel K, Hansen SB, *et al.* 2020. Ligand-recognizing motifs in plant LysM receptors are major determinants of specificity. *Science* **369**, 663–670.

Brini M, Marsault R, Bastianutto C, Alvarez J, Pozzan T, Rizzuto R. **1995**. Transfected aequorin in the measurement of cytosolic Ca^{2+} concentration ($[Ca^{2+}]_c$): a critical evaluation. *Journal of Biological Chemistry* **270**, 9896–9903.

Cao Y, Liang Y, Tanaka K, Nguyen CT, Jedrzejczak RP, Joachimiak A, Stacey G. **2014**. The kinase LYK5 is a major chitin receptor in *Arabidopsis* and forms a chitin-induced complex with related kinase CERK1. *eLife* **3**.

Capoen W, Sun J, Wysham D, *et al.* 2011. Nuclear membranes control symbiotic calcium signaling of legumes. *Proceedings of the National Academy of Sciences*, USA **108**, 14348–14353.

Carotenuto G, Chabaud M, Miyata K, Capozzi M, Takeda N, Kaku H, Shibuya N, Nakagawa T, Barker DG, Genre A. **2017**. The rice LysM receptor-like kinase OsCERK1 is required for the perception of short-chain chitin oligomers in arbuscular mycorrhizal signaling. *New Phytologist* **214**, 1440–1446.

Chabaud M, Genre A, Sieberer BJ, Faccio A, Fournier J, Novero M, Barker DG, Bonfante P. 2011. Arbuscular mycorrhizal hyphopodia and germinated spore exudates trigger Ca^{2+} spiking in the legume and nonlegume root epidermis. *New Phytologist* **189**, 347-55.

Charpentier M. **2018**. Calcium signals in the plant nucleus: origin and function. *Journal of Experimental Botany* **69**, 4165–4173.

Chiu CH, Paszkowski U. **2020**. Receptor-like kinases sustain symbiotic scrutiny. *Plant Physiology* **182**, 1597-1612.

Chiu CH, Roszak P, Orvošová M, Paszkowski U. 2022. Arbuscular mycorrhizal fungi induce lateral root development in angiosperms via a conserved set of MAMP receptors. *Current Biology* **32**, 4428–4437.

Choi J, Summers W, Paszkowski U. 2018. Mechanisms underlying establishment of arbuscular mycorrhizal symbioses. *Annual Review of Phytopathology* **56**, 135–160.

Cortese E, Moscatiello R, Pettiti F, *et al.* 2022. Monitoring calcium handling by the plant endoplasmic reticulum with a low-Ca^{2+}-affinity targeted aequorin reporter. *The Plant Journal* **109**, 1014–1027.

Costa A, Navazio L, Szabo I. **2018**. The contribution of organelles to plant intracellular calcium signalling. *Journal of Experimental Botany* **69**, 4175-4193.

De Vriese K, Costa A, Beeckman T, Vanneste S. **2018**. Pharmacological strategies for manipulating plant Ca^{2+} signalling. *International Journal of Molecular Sciences* **19**, 1506.

Delaux PM, Schornack S. 2021. Plant evolution driven by interactions with symbiotic and pathogenic microbes. *Science* **371**, eaba6605.

Dünser K, Schöller M, Rößling AK, *et al.* 2022. Endocytic trafficking promotes vacuolar enlargements for fast cell expansion rates in plants. *eLife* **11**, e75945.

Ehrhardt DW, Wais R, Long SR. 1996. Calcium spiking in plant root hairs responding to rhizobium nodulation signals. *Cell* **85**, 673-681.

Feng F, Sun J, Radhakrishnan GV, *et al.* 2019. A combination of chitooligosaccharide and lipochitooligosaccharide recognition promotes arbuscular mycorrhizal associations in *Medicago truncatula*. *Nature Communications* **10**, 5047.

Feng Y, Wu P, Liu C, *et al.* 2021. Suppression of LjBAK1-mediated immunity by SymRK promotes rhizobial infection in *Lotus japonicus*. *Molecular Plant* **14**, 1935–1950.

Francia D, Chiltz A, Lo Schiavo F, Pugin A, Bonfante P, Cardinale F. 2011. AM fungal exudates activate MAP kinases in plant cells in dependence from cytosolic Ca^{2+} increase. *Plant Physiology and Biochemistry* **49**, 963–969.

Genre A, Chabaud M, Balzergue C, *et al.* 2013. Short-chain chitin oligomers from arbuscular mycorrhizal fungi trigger nuclear Ca^{2+} spiking in *Medicago truncatula* roots and their production is enhanced by strigolactone. *New Phytologist* **198**, 190–202.

Genre A, Lanfranco L, Perotto S, Bonfante P. 2020. Unique and common traits in mycorrhizal symbioses. *Nature Reviews Microbiology* **18**, 649–660.

Ghahremani M, MacLean AM. 2021. Home sweet home: how mutualistic microbes modify root development to promote symbiosis. *Journal of Experimental Botany* **72**, 275–2287.

Gibelin-Viala C, Amblard E, Puech-Pages V, *et al.* 2019. The *Medicago truncatula* LysM receptor-like kinase LYK9 plays a dual role in immunity and the arbuscular mycorrhizal symbiosis. *New Phytologist* **223**, 1516–1529.

Giovannetti M, Mari A, Novero M, Bonfante P. 2015. Early *Lotus japonicus* root transcriptomic responses to symbiotic and pathogenic fungal exudates. *Frontiers in Plant Science* **6**, 480.

Grenzi M, Resentini F, Vanneste S, Zottini M, Bassi A, Costa A. 2021. Illuminating the hidden world of calcium ions in plants with a universe of indicators. *Plant Physiology* **187**: 550–571.

Greotti E, De Stefani D. 2020. Biosensors for detection of calcium. *Methods in Cell Biology* **155**: 337-368.

Kamal N, Mun T, Reid D, *et al.* 2020. Insights into the evolution of symbiosis gene copy number and distribution from a chromosome-scale *Lotus japonicus* Gifu genome sequence. *DNA Research* **27**, dsaa015.

Keinath NF, Waadt R, Brugman R, Schroeder JI, Grossmann G, Schumacher K, Krebs M. 2015. Live cell Imaging with R-GECO1 sheds light on flg22- and chitin-induced transient $[Ca^{2+}]_{cyt}$ patterns in *Arabidopsis*. *Molecular Plant* **8**, 1188–1200.

Kelner A, Leitão N, Chabaud M, Charpentier M, de Carvalho-Niebel F. 2018 Dual color sensors for simultaneous analysis of calcium signal dynamics in the nuclear and cytoplasmic compartments of plant cells. *Frontiers in Plant Science* **9**: 245.

Köster P, DeFalco T, Zipfel C. 2022. Ca^{2+} signals in plant immunity. *The EMBO Journal* **41**, e110741.

Kutschera A, Dawid C, Gisch N, *et al.* 2019. Bacterial medium-chain 3-hydroxy fatty acid metabolites trigger immunity in *Arabidopsis* plants. *Science* **364**, 178–181.

Lampropoulos A, Sutikovic Z, Wenzl C, Maegele I, Lohmann JU, Forner J. 2013. GreenGate - a novel, versatile, and efficient cloning system for plant transgenesis. *PLoS One* **8**, e83043.

Luo J, Chen L, Huang F, Gao P, Zhao H, Wang Y, Han S. 2020. Intraorganellar calcium imaging in Arabidopsis seedling roots using the GCaMP variants GCaMP6m and R-CEPIA1er. *Journal of Plant Physiology* **246–247**, 153127.

Małolepszy A, Mun T, Sandal N, *et al.* 2016. The LORE1 insertion mutant resource. *Plant Journal* **88**: 306-317.

Maillet F, Poinsot V, André O, *et al.* 2011. Fungal lipochitooligosaccharide symbiotic signals in arbuscular mycorrhiza. *Nature* **469**, 58–63.

Mehlmer N, Parvin N, Hurst CH, Knight MR, Teige M, Vothknecht UC. **2012**. A toolset of aequorin expression vectors for in planta studies of subcellular calcium concentrations in *Arabidopsis thaliana*. *Journal of Experimental Botany* **63**, 1751–1761.

Mittal, D., Mishra, S., Prajapati, R., Vadassery, J. 2020. Forward genetic screen using transgenic calcium reporter aequorin to identify novel targets in calcium signaling. *Journal of Visualized Experiments* **162**, e61259.

Miwa H, Sun J, Oldroyd GED, Downie JA. **2006**. Analysis of Nod-factor-induced calcium signaling in root hairs of symbiotically defective mutants of *Lotus japonicus*. *Molecular Plant-Microbe Interactions* **19**, 914–923.

Miyata K, Kozaki T, Kouzai Y, 2014. The bifunctional plant receptor, OsCERK1, regulates both chitin-triggered immunity and arbuscular mycorrhizal symbiosis in rice. *Plant & Cell Physiology* **55**, 1864–1872.

Monaghan J, Matschi S, Romeis T, Zipfel C. 2015. The calcium-dependent protein kinase CPK28 negatively regulates the BIK1-mediated PAMP-induced calcium burst. *Plant Signaling & Behavior* **10**, e1018497.

Morieri G, Martinez EA, Jarynowski A, Driguez H, Morris R, Oldroyd GED, Downie JA. **2013**. Host-specific Nod-factors associated with *Medicago truncatula* nodule infection differentially induce calcium influx and calcium spiking in root hairs. *New Phytologist* **200**, 656–662.

Moscatiello R, Sello S, Ruocco M, *et al.* 2018. The hydrophobin HYTLO1 secreted by the biocontrol fungus *Trichoderma longibrachiatum* triggers a NAADP-mediated calcium signalling pathway in *Lotus japonicus*. *International Journal of Molecular Sciences* **19**, 2596.

Mun T, Bachmann A, Gupta V, *et al.* 2016. Lotus Base: An integrated information portal for the model legume *Lotus japonicus*. *Scientific Reports* **6**, 39447.

Nakagawa T, Kaku H, Shimoda Y, Sugiyama A, Shimamura M, Takanashi K, Yazaki K, Aoki T, Shibuya N, Kouchi H. 2011. From defense to symbiosis: limited alterations in the kinase

domain of LysM receptor-like kinases are crucial for evolution of legume–Rhizobium symbiosis. *The Plant Journal* **65**, 169–180.

Nars A, Lafitte C, Chabaud M, *et al.* 2013. *Aphanomyces euteiches* cell wall fractions containing novel glucan-chitosaccharides induce defense genes and nuclear calcium oscillations in the plant host *Medicago truncatula*. *PLoS One* **8**, e75039.

Navazio L, Moscatiello R, Genre A, Novero M, Baldan B, Bonfante P, Mariani P. **2007**. A diffusible signal from arbuscular mycorrhizal fungi elicits a transient cytosolic calcium elevation in host plant cells. *Plant Physiology* **144**, 673–681.

Oldroyd GED. **2013**. Speak, friend, and enter: signalling systems that promote beneficial symbiotic associations in plants. *Nature Reviews Microbiology* **11**, 252–263.

Ottolini D, Calì T, Brini M. 2014. Methods to measure intracellular Ca^{2+} fluxes with organelle-targeted aequorin-based probes. *Methods in Enzymology* **543**, 21–45.

Platre MP, Satbhai SB, Brent L. *et al.* 2022. The receptor kinase SRF3 coordinates iron-level and flagellin dependent defense and growth responses in plants. *Nature Communications* **13**, 4445.

Radhakrishnan GV, Keller J, Rich MK, *et al.* 2020. An ancestral signalling pathway is conserved in intracellular symbioses-forming plant lineages. *Nature Plants* **6**, 280–289.

Ranf S, Eschen-Lippold L, Pecher P, Lee J, Scheel D. **2011**. Interplay between calcium signalling and early signalling elements during defence responses to microbe- or damage-associated molecular patterns. *The Plant Journal* **68**, 100–113.

R Core Team. 2022. R: A language and environment for statistical computing. R Foundation for Statistical Computing, Vienna, Austria. URL https://www.R-project.org/.

Resentini F, Grenzi M, Ancora D, Cademartori M, Luoni L, Franco M, Bassi A, Bonza MC, Costa A. **2021**. Simultaneous imaging of ER and cytosolic Ca^{2+} dynamics reveals long-distance ER Ca^{2+} waves in plants. *Plant Physiology* **187**, 603–617.

Ried MK, Banhara A, Hwu FY, Binder A, Gust AA, Höfle C, Hückelhoven R, Nürnberger T, Parniske M. 2019. A set of Arabidopsis genes involved in the accommodation of the downy mildew pathogen *Hyaloperonospora arabidopsidis*. *PLoS Pathogens* **15**, e1007747.

RStudio Team. 2020. RStudio: Integrated Development for R. RStudio, PBC, Boston, MA URL http://www.rstudio.com/.

Shaw SL, Long SR. **2003**. Nod Factor elicits two separable calcium responses in *Medicago truncatula* root hair cells. *Plant Physiology* **131**, 976–984.

Sieberer BJ, Chabaud M, Timmers AC, Monin A, Fournier J, Barker DG. 2009. A nuclear-targeted cameleon demonstrates intranuclear Ca^{2+} spiking in *Medicago truncatula* root hairs in response to rhizobial nodulation factors. *Plant Physiol*. **151**, 1197-206.

Sun J, Miller JB, Granqvist E, *et al.* 2015. Activation of symbiosis signaling by arbuscular mycorrhizal fungi in legumes and rice. *The Plant Cell* **27**, 823–838.

Thor K, Peiter E. **2014**. Cytosolic calcium signals elicited by the pathogen-associated molecular pattern flg22 in stomatal guard cells are of an oscillatory nature. *New Phytologist* **204**, 873–881.

Thor K, Jiang S, Michard E, *et al.* 2020. The calcium-permeable channel OSCA1.3 regulates plant stomatal immunity. *Nature* **585**, 569–573.

Tian, W., Hou, C., Ren, Z. *et al.* 2019. A calmodulin-gated calcium channel links pathogen patterns to plant immunity. *Nature* **572**, 131–135.

Verbon EH, Liberman LM. 2016. Beneficial microbes affect endogenous mechanisms controlling root development. *Trends in Plant Science* **21**, 218-229.

Volpe V, Carotenuto G, Berzero C, Cagnina L, Puech-Pagès V, Genre A. 2020. Short chain chito-oligosaccharides promote arbuscular mycorrhizal colonization in *Medicago truncatula*. *Carbohydrate Polymers* **1**, 229: 115505.

Wan J, Tanaka K, Zhang X-C, Son GH, Brechenmacher L, Nguyen THN, Stacey G. **2012**. LYK4, a lysin motif receptor-like kinase, is important for chitin signaling and plant innate immunity in Arabidopsis. *Plant Physiology* **160**, 396–406.

Wise AA, Liu Z, Binns AN. **2006**. Three methods for the introduction of foreign DNA into Agrobacterium. In: Wang K, ed. Methods in Molecular Biology. Agrobacterium Protocols. Totowa, NJ: Humana Press, 43–54.

Wu F, Chi Y, Jiang Z, *et al.* 2020. Hydrogen peroxide sensor HPCA1 is an LRR receptor kinase in *Arabidopsis*. *Nature* **578**, 577–581.

Yao P, Vanneste S, Navazio L, Van Breusegem F, Stael S. 2022. Chemical perturbation of chloroplast Ca^{2+} dynamics in *Arabidopsis thaliana* suspension cell cultures and seedlings. *Methods in Molecular Biology* **2494**, 149-158.

Yu X, Feng B, He P, Shan L. 2017. From chaos to harmony: responses and signaling upon microbial pattern recognition. *Annual Review of Phytopathology* **55**, 109-137.

Zhang X, Dong W, Sun J, Feng F, Deng Y, He Z, Oldroyd GED, Wang E. 2015. The receptor kinase CERK1 has dual functions in symbiosis and immunity signalling. *The Plant Journal* **81**, 258–267.

Zhang C, He J, Dai H, Wang G, Zhang X, Wang C, Shi J, Chen X, Wang D, Wang E. **2021**. Discriminating symbiosis and immunity signals by receptor competition in rice. *Proceedings of the National Academy of Sciences*, USA **118**, e2023738118.

Zipfel C, Oldroyd GED. **2017**. Plant signalling in symbiosis and immunity. *Nature* **543**, 328–33

Figure legends

Fig. 1. Monitoring of cytosolic and nuclear [Ca^{2+}] in root segments from composite plants of *L. japonicus* in response to different chitin-based oligomers. *L. japonicus* roots were transformed via *A. rhizogenes* with constructs encoding aequorin chimeras targeted to either the cytosol (A,C) or nucleus (B,D) and subcellular Ca^{2+} dynamics were measured after challenge with 10^{-7} M CO4 (dark blue), 10^{-6} M CO8 (green), 10^{-7} M mycLCOs (light blue) or with the same concentration of the solvents in which the compounds were dissolved (grey). In A-B, data are presented as means ± SE (shading) of n≥6 traces from at least 3 different composite plants (independent transformations). The arrow indicates the time of stimulus injection (time 0). In C-D, dots represent the maximum [Ca^{2+}] value for each trace in the time range of 1-18 minutes. Boxplots depicted on top of the panel (time) and at the right of the panel ([Ca^{2+}]) show the medians and the quartiles values.

Fig. 2. Pharmacological analyses of short-chain COs-induced intracellular Ca^{2+} fluxes in *L. japonicus* roots. Cytosolic [Ca^{2+}] (A,C) and nuclear [Ca^{2+}] (B,D) dynamics were monitored in root segments from composite plants challenged with 10^{-7} M CO4 after pre-treatment with either 1.5 mM $LaCl_3$ (dark violet), 2 mM EGTA (light violet), 50 µM CPA (light green), 10 µM VAC1 (dark green) or none (grey, either H2O or solvent control). In A-B, data are presented as means ± SE (shading) of n≥6 traces obtained from at least 3 different composite plants (independent transformation). In C-D, small dots represent the delta maximum cytosolic [Ca^{2+}] ($\Delta[Ca^{2+}]_{cyt}$) (C) and the delta integrated [Ca^{2+}] ($\Delta[Ca^{2+}]_{nuc}$) (D) for each trace in the time range of 2-20 minutes, while the big circles represent the mean. $\Delta[Ca^{2+}]$ was calculated by subtracting the mean of the resting [Ca^{2+}] in the pre-stimulus phase to each [Ca^{2+}] measurement value following the stimulus injection (arrow). The coloured vertical line shows the difference between the mean of each treatment and the control (horizontal grey line). Different letters indicate statistically significant differences among groups, according to Kruskal-Wallis test followed by Dunn's post-hoc correction (p-value <0.05).

Fig. 3. CO4-, CO8- and mycLCOs-induced nuclear Ca^{2+} responses in *L. japonicus* CSSP mutant backgrounds. Monitoring of nuclear [Ca^{2+}] in root segments from composite plants of *L. japonicus* wild-type (grey), *castor* (dark orange), *symrk* (light orange). Ca^{2+} measurements were conducted in response to 10^{-7} M CO4 (A-D), 10^{-6} M CO8 (E-H), 10^{-7} M mycLCOs (I-L). In A, E, I, data are presented as means ± SE (shading) of n≥6 traces from at least 3 different composite plants (independent transformation). Arrows indicate the time of stimulus injection (time 0). The dashed line separates phase 1 (0-8 minutes after stimulus) and phase 2 (8-30 minutes after stimulus). In B, F, J, dots represent the maximum [Ca^{2+}] for each trace in the whole run. In C, G, K, dots represent the integrated [Ca^{2+}] for each trace in the whole run and in the two different phases. In D, H, L, dots represent the Ca^{2+} transient width, in terms of the time interval in which [Ca^{2+}] exceeds the arbitrary threshold of 0.4 µM. The black line represents the median of each group. Different letters indicate statistically significant differences among groups, according to Kruskal-Wallis test followed by Dunn's post-hoc correction (p-value <0.05).

Fig. 4. Monitoring of nuclear Ca^{2+} in root atrichoblasts from *M. truncatula* root organ cultures expressing NupYC2.1. A,B,E,F show representative nuclear Ca^{2+} profiles (expressed as YFP/CFP FRET ratio) of individual cells from treated (10^{-7} M CO4) and untreated (control) root segments. CO4 treatment triggered intense oscillations (spiking) in nuclear Ca^{2+} levels. C,D,G,H show polynomial curves (orange) fitting the average values (dark grey) of the FRET traces from the responding cells (light grey) of two independent roots, treated (C,D) or not (G,H) with CO4. The polynomial curves of CO4-treated roots display an initial maximum within the first 8 minutes and a second less pronounced elevation in the following period. A minimum of 9 nuclei were imaged for each root.

Fig. 5. Monitoring of cytosolic and nuclear [Ca^{2+}] in root segments from composite plants of *L. japonicus cerk6*. Ca^{2+} measurements were conducted in the cytosol (A,C) and nucleus (B,D) in response to 10^{-7} M CO4 (A,C), 10^{-6} M CO8 (B,D). Data are presented as means ± SE (shading) of n≥3 traces from at least 3 responsive composite plants (independent transformation). The Ca^{2+}

responses measured in *cerk6* mutant background (purple) are compared with those obtained in the wild-type (grey) and *symrk* (orange), shown as moving average (dashed line). Only ~30% *cerk6* root samples displayed Ca^{2+} signals. Arrows indicate the time of stimulus injection (time 0). The dashed line separates phase 1 (0-8 minutes after stimulus) and phase 2 (8-30 minutes after stimulus).

Fig. 6. The effect of serial dilutions of CO4 on the induction of intracellular Ca^{2+} changes and on the activation of immunity marker genes in *L. japonicus* roots. In A, changes in free cytosolic and nuclear [Ca^{2+}] were measured in 5 mm-long root segments from composite plants of *L. japonicus* in Gifu wild-type in response to progressive dilutions of CO4 (10^{-6} M dark blue, 10^{-7} M light blue, 10^{-8} M teal, 10^{-9} M light teal). In A and C, data are presented as means ± SE (shading) of n≥3 traces from at least 3 different composite plants (independent transformation). Arrows indicate the time of stimulus injection (time 0). The dashed line separates phase 1 (0-8 minutes after stimulus) and phase 2 (8-30 minutes after stimulus). In B and C, dots represent the integrated [Ca^{2+}] for each trace in the two different phases. The black line represents the median of each group. In E, gene expression analysis by qRT-PCR of *LjChitinase* (Lj5g3v1961260), *LjRbohB-like* (Lj6g3v1549190), *LjWRKY70-like* (Lj1g3v1134110), *LjPRp27-like* (Lj5g3v2112200) relative to the two reference genes. *L. japonicus* Gifu seedlings were treated for 1 h with solvent control (white), 10^{-9} M CO4 (light teal) or 10^{-7} M CO4 (light blue) solutions. For each gene, expression is normalized to the control group average. Each dot represents a biological replicate, which is a pool of roots from 12 different plants. The black line represents the median. Different letters indicate statistically significant differences among groups according to Kruskal Wallis and Dunn's post hoc tests (B, D) or to ANOVA test followed by Tukey's post-hoc correction (E) (p-value<0.05).

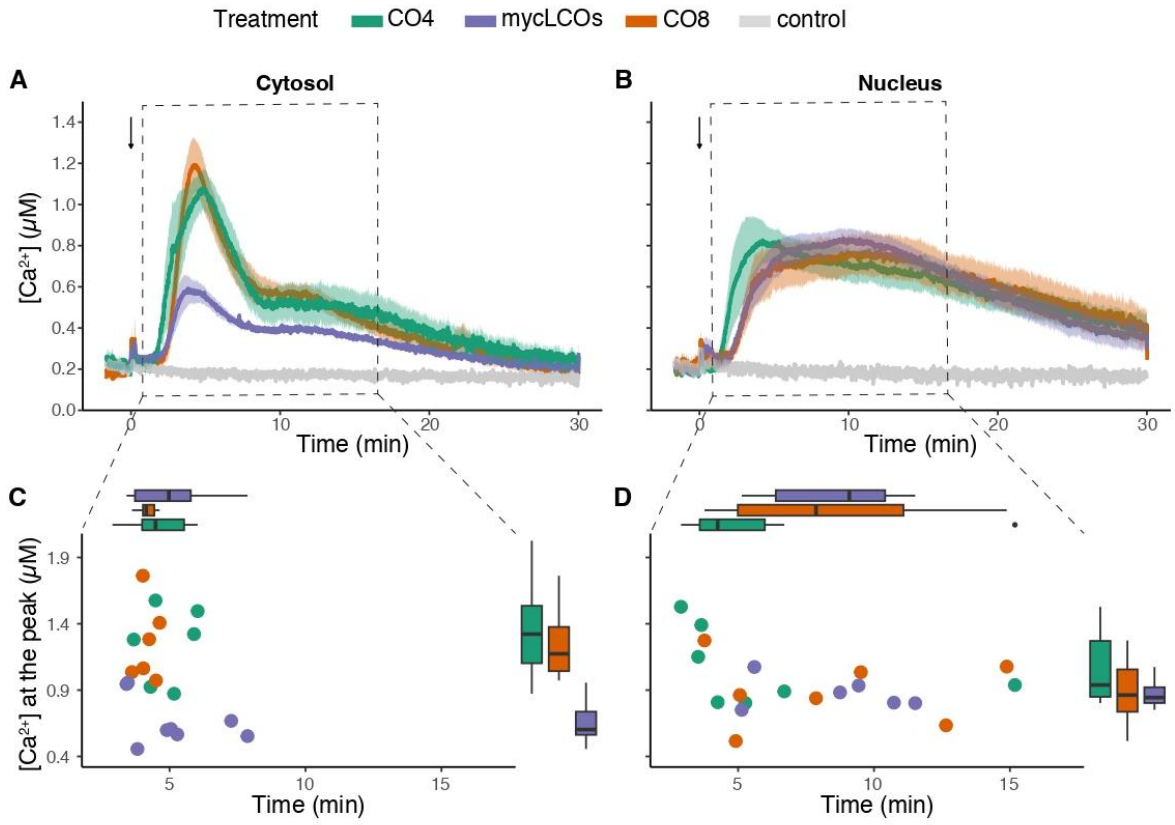

Fig. 1. Monitoring of cytosolic and nuclear free [Ca^{2+}] in 5 mm-long root segments from composite plants of *L. japonicus* in response to different chitin-based oligomers.
L. japonicus roots were transformed via *A. rhizogenes* with constructs encoding aequorin chimeras targeted to either the cytosol (A,C) or nucleus (B,D) and subcellular Ca^{2+} dynamics were measured after challenge with 10^{-7} M CO4 (dark blue), 10^{-6} M CO8 (green), 10^{-7} M mycLCOs (light blue) or with the same concentration of the solvents in which the compounds were dissolved (grey). In A-B, data are presented as means ± SE (shading) of n≥6 traces from at least 3 different composite plants (independent transformations). The arrow indicates the time of stimulus injection (time 0). In C-D, dots represent the maximum [Ca^{2+}] value for each trace in the time range of 1-18 minutes. Boxplots depicted on top of the panel (time) and at the right of the panel ([Ca^{2+}]) show the medians and the quartiles values.

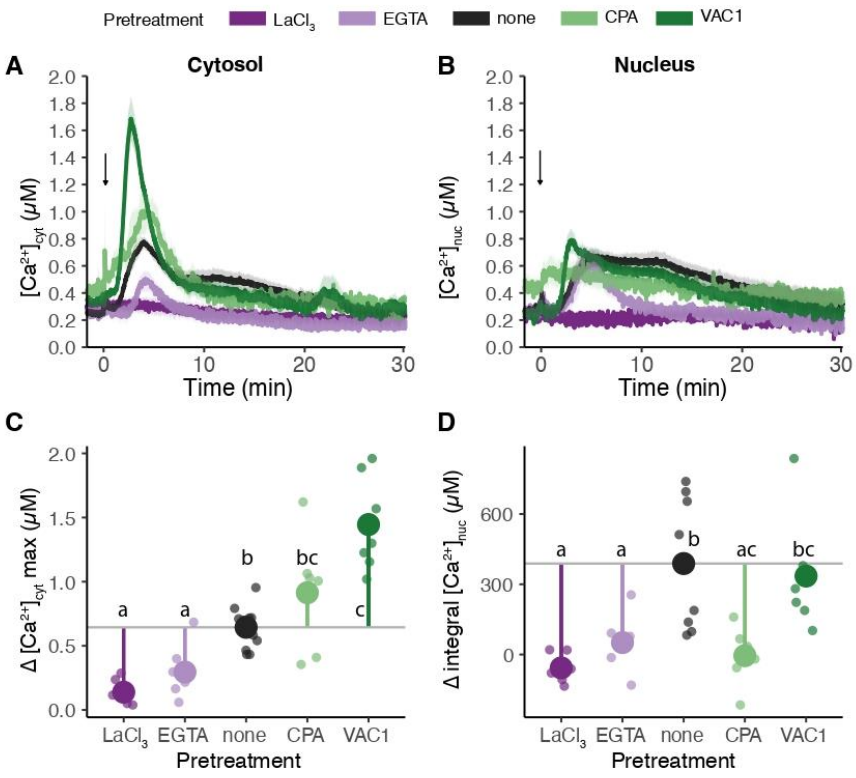

Fig. 2. Pharmacological analyses of short-chain COs-induced intracellular Ca^{2+} fluxes in *L. japonicus* roots.
Cytosolic [Ca^{2+}] (A,C) and nuclear [Ca^{2+}] (B,D) dynamics were monitored in root segments from composite plants challenged with 10^{-7} M CO4 after pre-treatment with either 1.5 mM $LaCl_3$ (dark violet), 2 mM EGTA (light violet), 50 µM CPA (light green), 10 µM VAC1 (dark green) or none (grey, either H_2O or solvent control). In A-B, data are presented as means ± SE (shading) of n≥6 traces obtained from at least 3 different composite plants (independent transformation). In C-D, small dots represent the delta maximum cytosolic [Ca^{2+}] ($\Delta[Ca^{2+}]_{cyt}$) (C) and the delta integrated [Ca^{2+}] ($\Delta[Ca^{2+}]_{nuc}$) (D) for each trace in the time range of 2-20 minutes, while the big circles represent the mean. $\Delta[Ca^{2+}]$ was calculated by subtracting the mean of the resting [Ca^{2+}] in the pre-stimulus phase to each [Ca^{2+}] measurement value following the stimulus injection (arrow). The coloured vertical line shows the difference between the mean of each treatment and the control (horizontal grey line). Different letters indicate statistically significant differences among groups, according to Kruskal-Wallis test followed by Dunn's post-hoc correction (p-value <0.05).

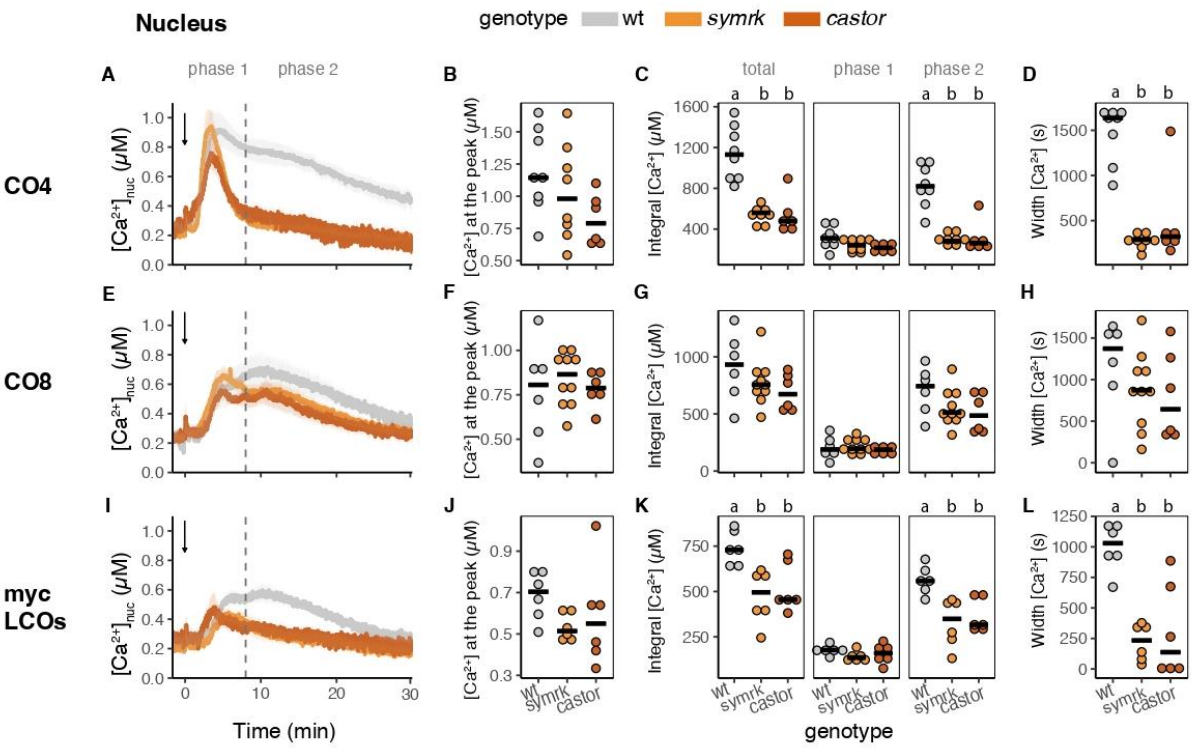

Fig. 3. CO4-, CO8- and mycLCOs-induced nuclear Ca^{2+} responses in *L. japonicus* CSSP mutant backgrounds.

Monitoring of nuclear [Ca^{2+}] in 5 mm-long root segments from composite plants of *L. japonicus* Gifu wild-type (grey), *castor* (dark orange), *symrk* (light orange). Ca^{2+} measurements were conducted in response to 10^{-7} M CO4 (A-D), 10^{-6} M CO8 (E-H), 10^{-7} M mycLCOs (I-L). In A, E, I, data are presented as means ± SE (shading) of n≥6 traces from at least 3 different composite plants (independent transformation). Arrows indicate the time of stimulus injection (time 0). The dashed line separates phase 1 (0-8 minutes after stimulus) and phase 2 (8-30 minutes after stimulus). In B, F, J, dots represent the maximum [Ca^{2+}] for each trace in the whole run. In C, G, K, dots represent the integrated [Ca^{2+}] for each trace in the whole run and in the two different phases. In D, H, L, dots represent the Ca^{2+} transient width, in terms of the time interval in which [Ca^{2+}] exceeds the arbitrary threshold of 0.4 μM. The black line represents the median of each group. Different letters indicate statistically significant differences among groups, according to Kruskal-Wallis test followed by Dunn's post-hoc correction (p-value <0.05).

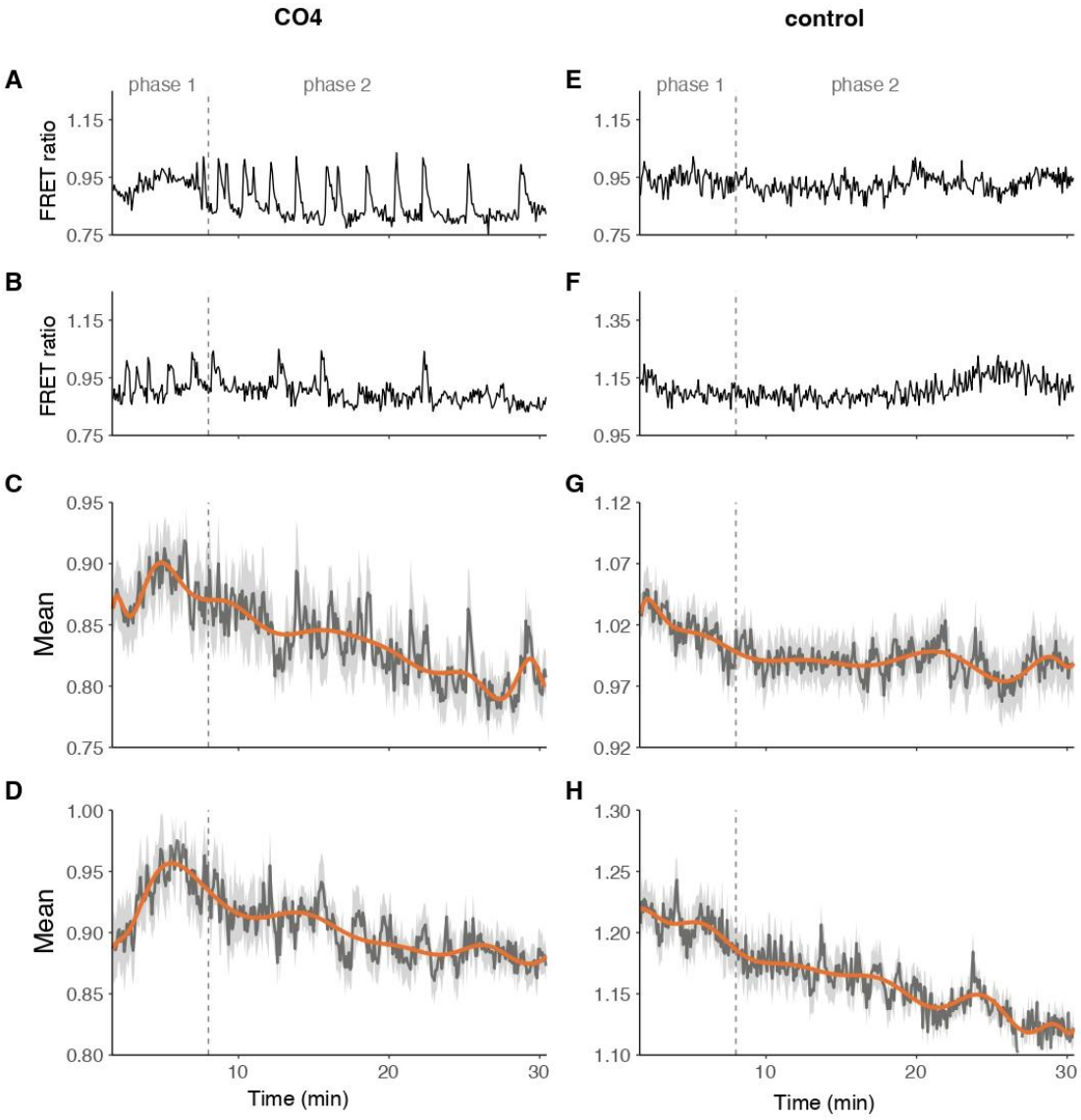

Fig. 4. Monitoring of nuclear Ca^{2+} in root atrichoblasts from *M. truncatula* root organ cultures expressing NupYC2.1.
A,B,E,F show representative nuclear Ca^{2+} profiles (expressed as YFP/CFP FRET ratio) of individual cells from treated (10^{-7} M CO4) and untreated (control) root segments. CO4 treatment triggered intense oscillations (spiking) in nuclear Ca^{2+} levels. C,D,G,H show polynomial curves (orange) fitting the average values (dark grey) of the FRET traces from the responding cells (light grey) of two independent roots, treated (C,D) or not (G,H) with CO4. The polynomial curves of CO4-treated roots display an initial maximum within the first 8 minutes and a second less pronounced elevation in the following period. A minimum of 9 nuclei were imaged for each root.

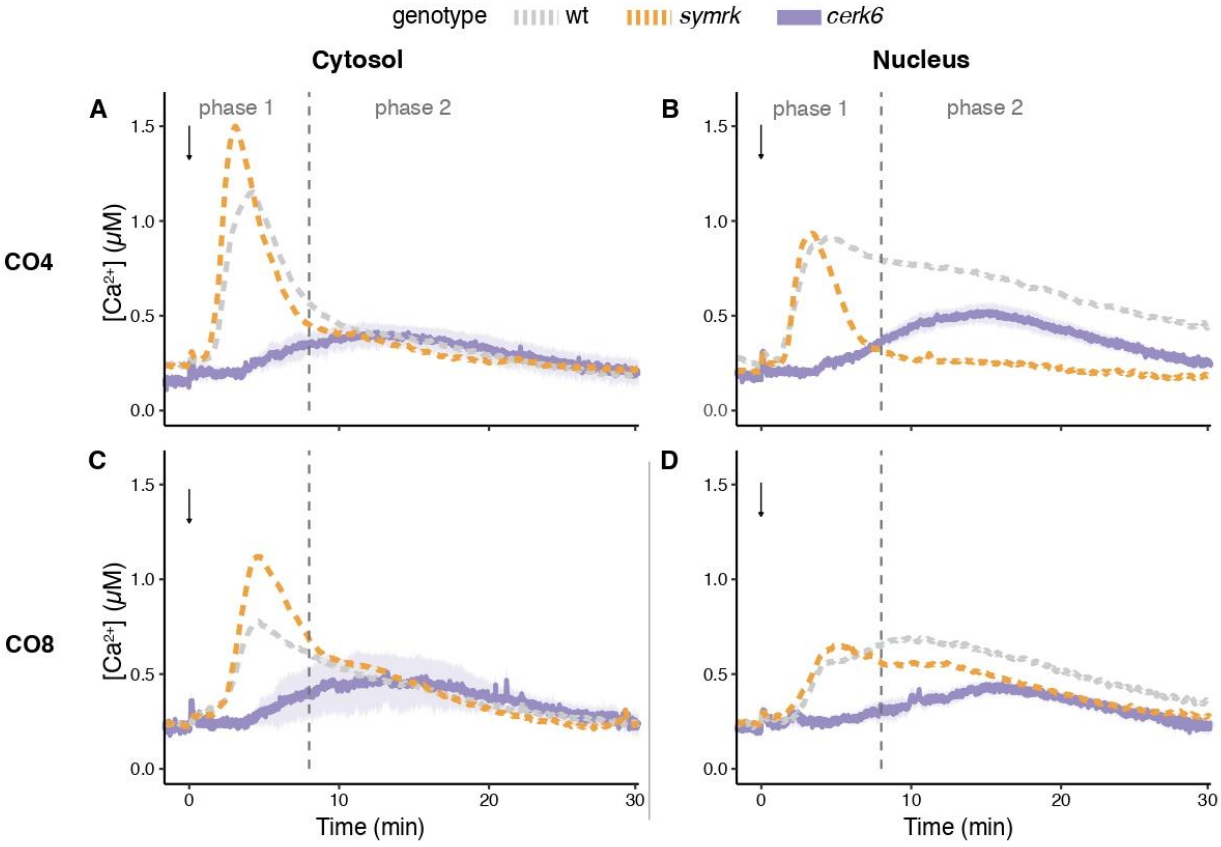

Fig. 5. Monitoring of free cytosolic and nuclear [Ca^{2+}] in 5 mm-long root segments from composite plants of *L. japonicus cerk6* (purple).
Ca^{2+} measurements were conducted in the cytosol (A,C) and nucleus (B,D) in response to 10^{-7} M CO4 (A,C), 10^{-6} M CO8 (B,D). Data are presented as means ± SE (shading) of n≥3 traces from at least 3 responsive composite plants (independent transformation). The Ca^{2+} responses measured in the Gifu wild-type (grey) and *symrk* (light orange) are shown as moving average (dashed line) for comparison. Arrows indicate the time of stimulus injection (time 0). The dashed line separates phase 1 (0-8 minutes after stimulus) and phase 2 (8-30 minutes after stimulus).

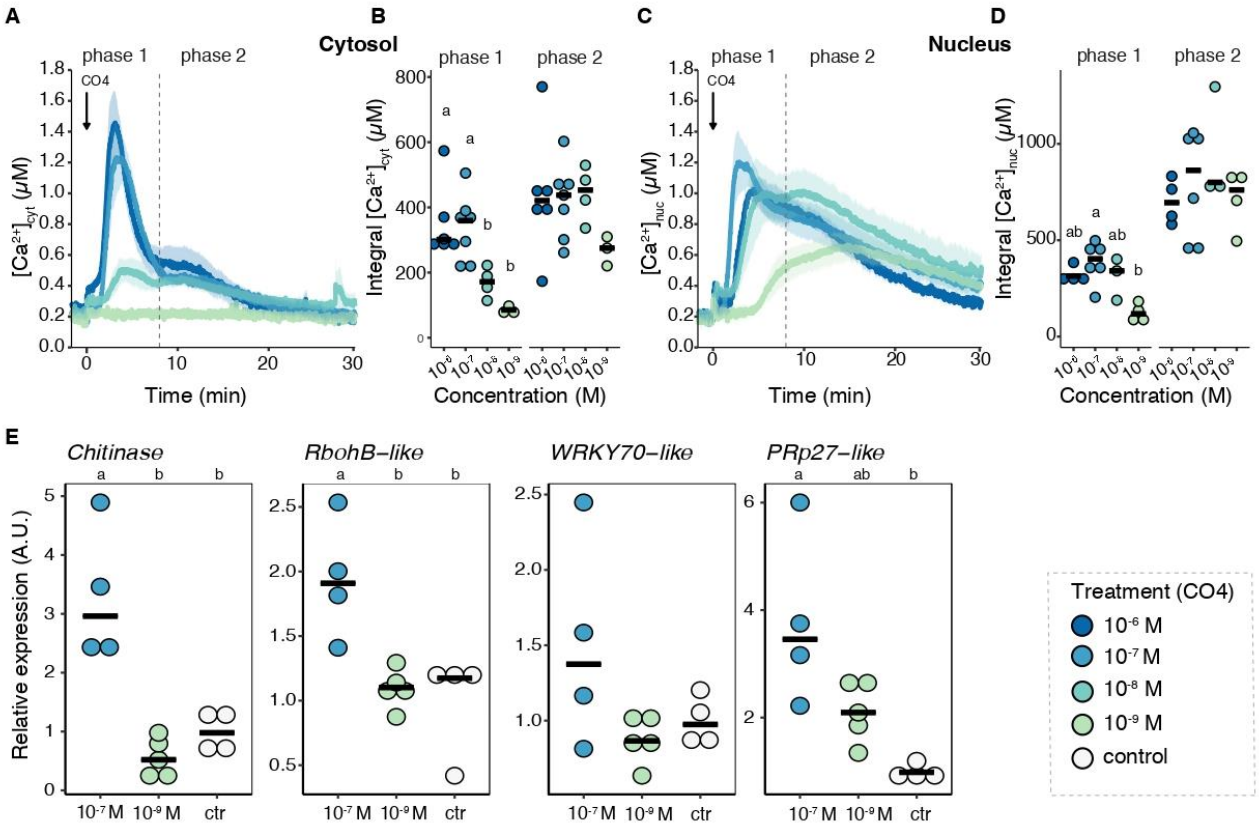

Fig. 6. The effect of serial dilutions of CO4 on the induced intracellular Ca^{2+} changes (A-D) and on the activation of immunity marker genes (E).
In A, changes in free cytosolic and nuclear [Ca^{2+}] were measured in 5 mm-long root segments from composite plants of *L. japonicus* in Gifu wt in response to progressive dilutions of CO4 (10^{-6} M dark blue, 10^{-7} M light blue, 10^{-8} M teal, 10^{-9} M light teal). In A and C, data are presented as means ± SE (shading) of n≥3 traces from at least 3 different composite plants (independent transformation). Arrows indicate the time of stimulus injection (time 0). The dashed line separates phase 1 (0-8 minutes after stimulus) and phase 2 (8-30 minutes after stimulus). In B and C, dots represent the integrated [Ca^{2+}] for each trace in the two different phases. The black line represents the median of each group. In E, gene expression analysis by qRT-PCR of *LjChitinase* (Lj5g3v1961260), *LjRbohB-like* (Lj6g3v1549190), *LjWRKY70-like* (Lj1g3v1134110), *LjPRp27-like* (Lj5g3v2112200) relative to the two reference genes. *L. japonicus* Gifu seedlings were treated for 1 h with solvent control (white), 10^{-9} M CO4 (light teal) or 10^{-7} M CO4 (light blue) solutions. For each gene, expression is normalized to the control group average. Each dot represents a biological replicate, which is a pool of roots from 12 different plants. The black line represents the median. Different letters indicate statistically significant differences among groups according to Kruskal Wallis and Dunn's post hoc tests (B, D) or to ANOVA test followed by Tukey's post-hoc correction (E) (p-value<0.05).